Performance of Low-Complexity Spectrally Selective One-Dimensional Mirrors for Photovoltaic Thermal Management

Preprint

Ian M. Slauch and Vivian E. Ferry
University of Minnesota

Michael G. Deceglie and Timothy J. Silverman
National Renewable Energy Laboratory

Presented at the 2018 World Conference on Photovoltaic Energy Conversion (WCPEC-7)
Waikoloa, Hawaii
June 10–15, 2018

Suggested Citation
Slauch, I.M., M.G. Deceglie, T.J. Silverman, and V.E. Ferry. 2018. "Performance of Low-Complexity Spectrally Selective One-Dimensional Mirrors for Photovoltaic Thermal Management: Preprint." Golden, CO: National Renewable Energy Laboratory. NREL/CP-5K00-71621.

NREL is a national laboratory of the U.S. Department of Energy
Office of Energy Efficiency & Renewable Energy
Operated by the Alliance for Sustainable Energy, LLC

This report is available at no cost from the National Renewable Energy Laboratory (NREL) at www.nrel.gov/publications.

Conference Paper
NREL/CP-5K00-71621
August 2018

Contract No. DE-AC36-08GO28308

NOTICE

This work was authored by the National Renewable Energy Laboratory, operated by Alliance for Sustainable Energy, LLC, for the U.S. Department of Energy (DOE) under Contract No. DE-AC36-08GO28308. Funding provided by U.S. Department of Energy Office of Energy Efficiency and Renewable Energy Solar Energy Technologies Office. The views expressed in the article do not necessarily represent the views of the DOE or the U.S. Government. The U.S. Government retains and the publisher, by accepting the article for publication, acknowledges that the U.S. Government retains a nonexclusive, paid-up, irrevocable, worldwide license to publish or reproduce the published form of this work, or allow others to do so, for U.S. Government purposes.

Cover Photos by Dennis Schroeder: (left to right) NREL 26173, NREL 18302, NREL 19758, NREL 29642, NREL 19795.

Performance of Low-Complexity Spectrally Selective One-Dimensional Mirrors for Photovoltaic Thermal Management

Ian M. Slauch[1], Michael G. Deceglie[2], Timothy J Silverman[2], and Vivian E. Ferry[1]

[1]University of Minnesota Department of Chemical Engineering and Materials Science, 421 Washington Ave SE, Minneapolis, MN 55455, USA

[2]National Renewable Energy Laboratory, Golden, CO 80401, USA

***Abstract* — Operation at elevated temperatures is detrimental to the performance of crystalline Si solar modules. One method of reducing module operating temperature is selective reflection of sub-bandgap photons, which can otherwise only be absorbed parasitically. We numerically optimize the design of a series of multilayer photonic mirrors based on real materials using a previously developed optimization routine. Combined ray tracing and finite element simulations reveal the ability of each mirror to increase energy yield and decrease operating temperature. The best design outperforms a conventional glass antireflection coating, contains only nine layers, and maintains performance regardless of geographic location.**

***Index Terms* — cooling, photonic structures, solar cells, solar modules, spectrally selective reflection.**

I. Introduction

All common solar cell materials, including crystalline Si, experience decreased efficiency with increased operating temperature. For c-Si, efficiency drops by ~0.4 %/K and, when encapsulated in a module, the cell operates 20 - 30 K above ambient under sunny conditions. In addition to carrier recombination, thermalization, and Ohmic loss, one major source of excess heat in a module is parasitic absorption of sub-bandgap radiation [1], which for c-Si under AM1.5 radiation, represents ~20% of total incident power. Here, our strategy is to design one-dimensional multilayer dielectric mirrors capable of lowering module operating temperature by reflecting sub-bandgap radiation.

In the best-case scenario, such a multilayer mirror would have two key features. It would firstly be highly spectrally selective, not only reflecting all light below the bandgap, but transmitting all light above the bandgap, potentially improving anti-reflection. Secondly, it would maintain spectral-selectivity at all angles of incidence. In a realistic mirror based on thin-film stacks, angle dependence in particular requires careful design, as the reflection features associated with the necessary spectral selectivity blue-shift as angle of incidence increases. Previously, we have shown [2] that consideration of the full range of angles of incidence, even when most sunlight is incident at lower angles, is important to achieve enhanced energy yield across a full year.

A further consideration is that if a mirror is placed at the outer module interface between the cover glass and air, then it replaces a conventional antireflection coating (ARC). A conventional ARC increases module temperature relative to an uncoated module by increasing waste heat from parasitic absorption and thermalization. Our previous mirror designs [2] and those of others [3] have shown that mirrors with structures based on Bragg stacks, including aperiodic structures derived from Bragg stacks, can offer better antireflection than a conventional ARC while still decreasing module operating temperature. However, these mirrors require many thin film layers to create a reflection band in the sub-bandgap region. Mirror designs with fewer layers will be cheaper and easier to fabricate, making them potentially more cost-effective than a conventional ARC while still providing sub-bandgap reflection at all angles of incidence.

In this paper, we consider the trade-off between limiting complexity (i.e. number of layers) in spectrally selective mirror designs and improving mirror performance both optically (transmission above bandgap) and thermally (reflection sub-bandgap and module temperature reduction). A mirror with a given number of layers and given material for each layer thickness is optimized via minimization of an objective function that captures the optical and thermal benefit [2]. After layer thickness optimization, we employ a needle-insertion algorithm [4]-[5] to insert new layers into the mirror. Full-year simulations of module temperature and output power are then performed using an opto-electro-thermal model described in [6], from which we determine the relative improvement in energy yield offered by a given mirror compared to both a baseline module without the mirror and a module with a conventional ARC. We additionally decompose this energy benefit into a thermal part due to sub-bandgap reflection and an optical part due to above bandgap transmission.

We compare the results of each mirror as a function of the number of its layers to determine the point at which addition of another needle no longer improves its performance. We discuss the magnitude of the total benefit achieved by these mirrors, and in particular we examine the possibility of spectral-selectivity in a low-complexity design. We then take one mirror which we determine to strike a balance between complexity and performance and simulate it using weather and irradiance conditions characteristic of dozens of locations across the continental United States.

II. Methods

A. Materials

Our optimization routine uses the refractive index dispersion present in real materials. We select five visibly transparent

dielectrics to form the material library for our mirrors: MgF_2, SiO_2, SiN_x, Al_2O_3, and ZrO_2. For MgF_2, we use the refractive index values given in [7], which are the result of a Kramers-Kronig consistent analysis on thin film MgF_2 deposited by evaporation at 300°C. The refractive indices of SiO_2, SiN_x, Al_2O_3, and ZrO_2 were extracted from spectroscopic ellipsometry measurements of thin films on Si substrates deposited at the Minnesota Nano Center as described below. For the module cover glass, we use the data from [8] and for air we take n = 1.

SiO_2, and SiN_x were deposited by plasma enhanced chemical vapor deposition (PECVD). For SiO_2, precursor gases were 200 sccm 2% SiH_4/98% He and 450 sccm N_2O and the deposition temperature was 250°C. For SiN_x, precursor gases were 200 sccm 2% SiH_4/98% He, 740 sccm N_2, and 2.0 sccm NH_3 and the deposition temperature was 340°C. For both SiO_2 and SiN_x, RF power was 20 W and the total chamber pressure was 900 mTorr.

Al_2O_3 and ZrO_2 were deposited by atomic layer deposition (ALD). For Al_2O_3, precursors were trimethylaluminum and water vapor, and the deposition temperature was 180°C. For ZrO_2, precursors were tetrakis(dimethylamino)zirconium and water vapor, and the deposition temperature was 250°C.

Spectroscopic ellipsometry was performed using a JA Woolam Vase Ellipsometer. Psi-delta measurements were taken at angles of 65, 70, and 75 degrees and at wavelengths 300 – 1100 nm at 20 nm (SiO_2, SIN_x, Al_2O_3) or 10 nm (ZrO_2) intervals. Each film was modelled using a Cauchy fit for the real index. For ZrO_2, a better fit to the psi-delta data was obtained with the addition of an Urbach absorption tail, [9] however for other films we take the imaginary index to be zero at all wavelengths considered. Furthermore, since the mirror optimization and optical modeling require refractive index data into the near infrared portion of the spectrum, we extrapolate the Cauchy fit out to 2500 nm. While the real dispersion in our films may not be approximated by the Cauchy model up to such long wavelengths, any deviations would be most severe at the longest wavelengths where the amount of solar power is the least. Therefore, the extrapolation is unlikely to cause meaningful error in either the optimization or simulation. The refractive indices of all films used for mirror design are shown in Fig. 1.

B. Mirror Design Optimization

Optimization was carried out via minimization of the objective function described in [2]. Briefly, this optimization method considers the thickness of each layer in the mirror to be the set of independent variables subject to optimization. The superstrate material for all mirrors discussed in this paper is air, and the substrate material is glass. The transfer matrix method is used to calculate reflection at wavelengths between 300 and 2500 nm and at angles of incidence between 0 and 89 degrees. Reflection values versus angle are weighted based on the expected total energy received for Golden, CO on a module at latitude tilt, as given in [2]. The final objective function value is the sum of two parts: estimated optical and thermal benefits compared to a module with no mirror.

The optical benefit for the objective function is based on the ratio of the currents produced in the module with and without the mirror. The current is calculated as the number of carriers extracted in (1) and the optical benefit is given in (2).

$$I = \int_{300}^{1100} \left(1 - R_w(\lambda)\right) \cdot IQE(\lambda) \cdot \Phi_{AM1.5}(\lambda)\, d\lambda \quad (1)$$

$$Opt\%_{obj} = 100\% \cdot (I/I_{baseline} - 1) \quad (2)$$

R_w are the weighted reflection values, IQE is the Si internal quantum efficiency, $\Phi_{AM1.5}$ is the photon flux of the AM1.5G spectrum, and $I_{baseline}$ is the result of (1) for the case without the mirror.

The thermal benefit is dependent on the difference in sub-bandgap power reflected by the interface with and without the mirror, given by (3) and (4). Equation (3) represents the sub-bandgap power reflected from the module. The percentage benefit in (4) assumes a 30 W/K conversion factor, representing a 1K increase in operating temperature for every 30 W increased power dissipation in the module. This conversion factor was determined by observing the temperature increase of a c-Si module under 1000 W/m^2 illumination [2]. Equation (4) also assumes a module power temperature coefficient of 0.39 %/K (decreased power at elevated temperature).

$$P = \int_{1100}^{2500} R_w(\lambda)\, P_{AM1.5}(\lambda)\, d\lambda \quad (3)$$

$$Thermal\ \%_{obj} = \frac{P - P_{baseline}}{30\ ^W/_K} \cdot 0.39\ ^{\%}/_K \quad (4)$$

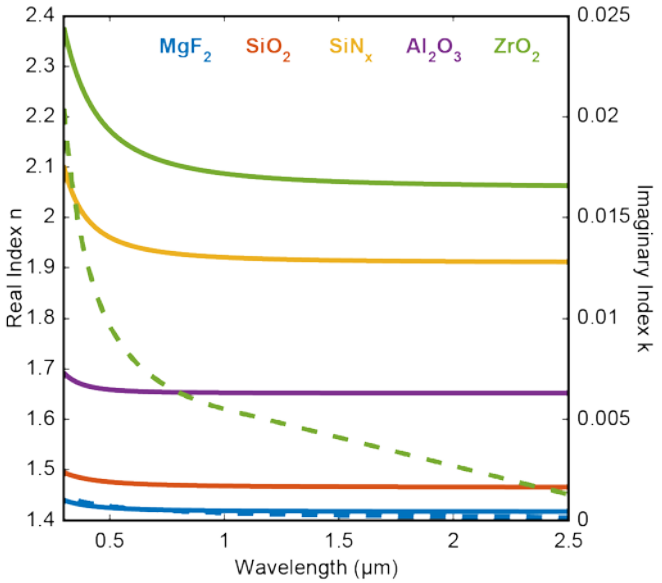

Fig. 1. Refractive indices of all materials used in any mirror. The data for MgF_2 is taken from [7], other material indices are extracted from spectroscopic ellipsometry. Solid lines indicate the real index while dashed lines indicate the imaginary index.

After layer thickness optimization, a needle insertion algorithm [5] checks which of the materials in the library would lead to the greatest decrease in the objective function value if

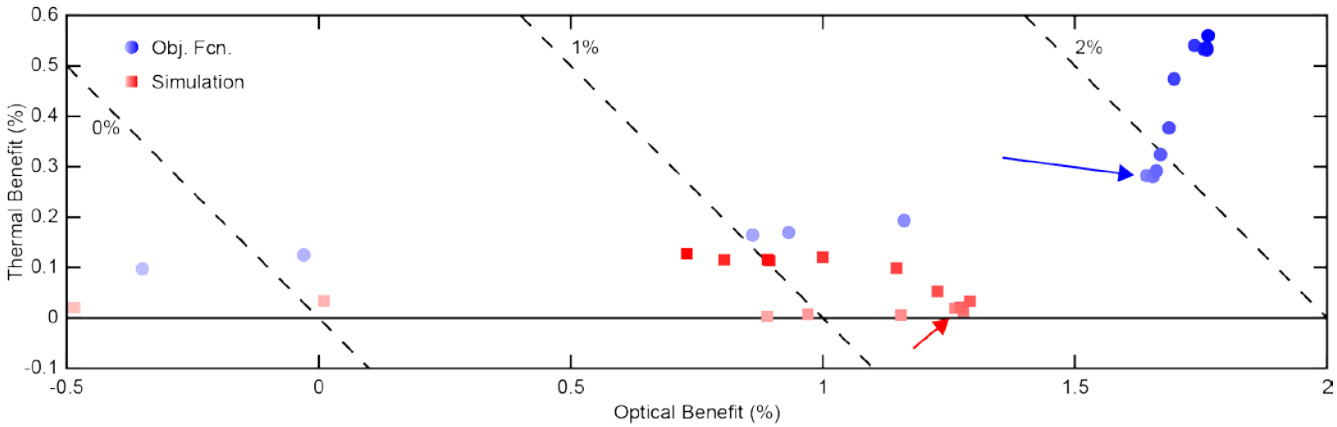

Fig. 2 Objective function values (blue circles) and simulation results (red squares) of mirrors 0-15. The opacity of the color indicates the iteration number; deeper colors are later iterations. The total benefit is the sum of the thermal and optical benefits. Lines of equal total benefit are plotted as dotted lines. For both the objective function and simulations, results are percentage improvements over a module with the glass ARC. The arrows denote the 5th iteration of the mirror (considered in more detail elsewhere in the paper).

inserted into the mirror. The location of insertion is determined by estimation of the gradient of the objective function with respect to insertion of a 0.1 nm thick layer, and choosing the insertion location corresponding to the estimated steepest descent. The magnitude of the benefit of the needle is determined after full reoptimization of all layer thicknesses with the needle included. The objective function is continuous with respect to insertion or deletion of very thin layers, and any layers that are set to ~1 nm or less during optimization are manually deleted afterwards and their objective function values are recalculated.

C. Opto-Electro-Thermal Simulations

Full-year opto-electro-thermal simulations are performed according to [6]. Module optical response is determined via a ray-tracing method that accounts for thin-film interference effects [10]. This optical response, along with characteristic weather and irradiance data, are used in a finite element model which calculates module temperature and output power. To simulate modules in a variety of geographic locations, weather data are taken from Typical Meteorological Year (TMY) data sets [11], and solar position and angle of incidence with respect to the module are calculated using the NREL Solar Position Algorithm [12]. Sky and ground temperatures required for the simulation are estimated using TMY data according to the supplemental information of [2].

As with the objective function, simulation results are compared to a baseline case with no mirror present, and the energy advantage is broken down into thermal and optical components. From the time series of module temperature ($T(t)$) and power ($W(t)$) at time t, the thermal advantage ($\Delta W_T(t)$) is calculated from (5).

$$\Delta W_T(t) = \Delta T(t) \cdot 0.39\,{}^{\%}/_{K} \cdot W_{baseline}(t) \qquad (5)$$

The Δ refers to the difference between the module with the mirror and the baseline at a given time step. The optical advantage ($\Delta W_O(t)$) is calculated from (6).

$$\Delta W_O(t) = \Delta W(t) - \Delta W_T(t) \qquad (6)$$

The total thermal and optical advantages are the ratios of the sums of ΔW_T and ΔW_O over time to the sum of baseline power over time.

All mirrors discussed in this paper are simulated at a module tilt of 20°. The angle-weighting used in optimization assumed a latitude tilt module in Golden, CO (40° tilt), and so the simulated modules experience a different angular distribution of sunlight than assumed during optimization. However, as can be seen in the supplemental information of [2], changing the angle weighting to reflect a new tilt or geographic location changes optimal layer thickness by ~1% or less, so the objective function is still a predictor of simulation results.

TABLE I
LAYER COUNTS FOR ALL MIRRORS

Mirror No.	0	1	2	3	4	5	6	7
No. of Layers	2	4	5	6	8	9	11	12
Mirror No.	8	9	10	11	12	13	14	15
No. of Layers	14	16	17	17	20	19	21	21

III. RESULTS AND DISCUSSION

A. Mirror Optimization and Objective Function Values

Optimization began with an initial condition of a MgF_2 layer on a SiO_2 layer on a glass substrate, with each layer having approximately quarter-wave optical thickness at 1600 nm. Repeated steps of layer thickness optimization followed by needle insertion were completed until sixteen different mirrors were designed, one for each layer thickness optimization step. The mirrors are numerically labelled according to the number of needle insertion steps that were performed to reach their layer structure. The first mirror is the optimized MgF_2/SiO_2

structure, labelled "0" since there are no needle insertion steps required to reach this structure. In total, 15 needle insertion steps were completed to give the sixteen different mirrors. Objective function values were tracked for each mirror, with the results shown in Fig. 2, and the layer count of each mirror is given in Table 1. While these mirrors represent optimal designs according to the objective function given the available library of materials, if different materials are used, then the designs will change and the objective function values may not be the same.

In general, needle insertion adds two layers to the mirror, one for the needle itself and one more because the needle splits a previously existing layer in two. However, after layer thickness optimization, some layers may end at near-zero thickness, thus sometimes only one layer is added to the mirror between optimization steps. Between steps 11 and 12, three layers are added, since a layer which earlier had near-zero thickness ended with appreciable thickness after step 12. Between steps 10 and 11 and steps 14 and 15, the layer count did not increase since two additional layers had near-zero thickness after optimization. These steps amount to a change in the materials or the material order of the mirror. Importantly, if needle insertion and layer thickness optimization are applied to mirror 15, the resulting mirror has the same materials in the same order, with only slightly different thicknesses and a very similar objective function value. Therefore, we chose not to continue needle insertion after mirror 15.

Although the optimization is performed relative to a baseline solar module with uncoated front glass, the relative improvements in Fig. 2 are shown compared to a module with a conventional glass ARC (99 nm porous SiO_2, index data given by [14]), as representative of what a multilayer mirror would likely replace on the front interface.

From the objective function values in Fig. 2 (blue circles), all mirrors act primarily as antireflection coatings. However, only from mirror 6 onwards does the thermal benefit increase substantially, while the optical benefit stays mostly the same. We offer two reasons for this trend during optimization. The first is that, without using gradient index or moth-eye effects [13], the double layer coating of mirror 0 cannot provide antireflection over the entire band from 300 – 1100 nm, while the four, five, six, eight, or nine layer structures of mirrors 1-5, respectively can increase the bandwidth of effective antireflection. Second, from previous simulations [2] on ideal ARCs at the air/glass interface, a >7% optical benefit is possible if all light is transmitted, while only a slightly greater than 1% thermal benefit is possible if all sub-bandgap light is reflected. Furthermore, the optical penalty for increasing reflection above the bandgap is severe. Therefore, if a mirror is not sufficiently complex to offer spectral-selectivity, it is better that it be an antireflection coating versus a sub-bandgap reflector.

B. Simulation Results of Mirrors 0 – 15 and Comparison to a Conventional Glass ARC

The performance of the same mirrors was then calculated using the opto-electro-thermal simulation method. Mirrors 0-15 were simulated using TMY data for Denver International Airport. The module tilt angle was 20 degrees. Simulation results are shown as red squares in Fig. 2 and, like the objective function values, are shown as percentage improvements compared to a module with a conventional glass ARC.

This objective function assumes that all light transmitted above the bandgap through the interface at which the mirror is placed reaches the cell and is absorbed in the cell, and that all transmitted sub-bandgap light is absorbed parasitically. These assumptions neglect the presence of other interfaces in the module, and in particular ignore the possibility of absorption in the encapsulant, especially at UV wavelengths. Furthermore, with increased module current, more heat is generated via electronic losses, which are not accounted for by the objective function. The effect of these is that the simulations of mirrors are consistently less beneficial thermally than predicted by the objective function.

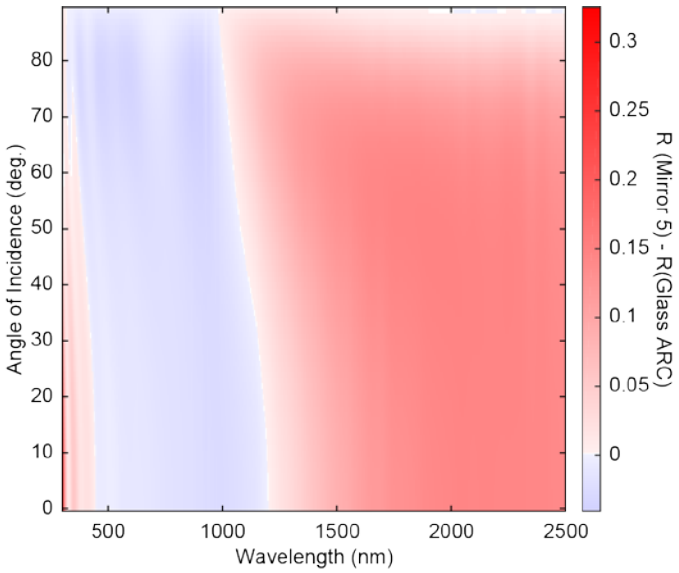

Fig. 3 Net reflection of mirror 5, compared to the air/glass ARC interface. Blue shades indicate that mirror 5 reflects less light than the bare air/glass ARC interface for a given wavelength and angle of incidence; red shades indicate that mirror 5 reflects more light than the air/glass ARC interface. Zero degrees corresponds to normal incidence.

While the mirrors all have a lower simulated thermal benefit than predicted by the objective function, all mirrors except mirror 0 have a higher optical and thermal benefit than the conventional glass ARC. These mirrors therefore allow their modules to produce more power and operate at lower temperatures than a module with a conventional ARC.

Based on these results, mirror 5 was designated as the best overall mirror in terms of achieving the highest total benefit with a relatively small number of layers in the structure. Table 2 shows the materials and layer thicknesses of mirror 5; layer 1 is adjacent to air and layer 9 is adjacent to the cover glass. The net reflection of mirror 5, i.e. the difference in reflection between mirror 5 and the air/glass ARC interface is plotted in Fig. 3. Blue colors correspond to wavelengths and angles of incidence where the mirror is antireflective, red colors correspond to

TABLE II
DETAILS OF MIRROR 5

Layer No.	Material	Thickness (nm)
1	MgF_2	117.8
2	ZrO_2	20.8
3	Al_2O_3	23.2
4	ZrO_2	116.9
5	Al_2O_3	20.3
6	SiN_x	37.9
7	SiO_2	41.8
8	SiN_x	12.0
9	SiO_2	207.1

regions where reflection is increased. As shown, the mirror is almost entirely antireflective in the region 300 – 1100 nm, except at low angles and wavelengths near 300 nm, and at high angles near 1100 nm. The mirror exhibits the required spectral selectivity at all angles of incidence. Since these mirrors are not based on Bragg-stack designs, they do not possess a well-defined reflection band with a sharp turn-on between transmission and reflection. A Bragg-stack-like design would have greater reflection in the sub-bandgap region, especially at shorter wavelengths where there is more incident spectral power. But, such a design would require dozens of layers, and may not be simple to fabricate.

Notably, the optical objective function value and optical simulation result do not closely agree starting at mirror 5 and continuing to mirror 15. The more complex mirrors all have objective function values giving over 4% optical improvement, while they simulated at no better than ~3.6% improvement optically. The discrepancy likely arises due to the more complex mirrors reducing reflection in the region <350 nm. While this increases the optical benefit in the objective function, the encapsulant used in the module simulations does not transmit any of this light to the cell. Therefore, in the simulation, mirror transmission <350 nm is not beneficial in the simulation.

C. Simulations Across the Continental United States

To further demonstrate the performance of mirror 5, we simulate both mirror 5 and the glass ARC at 47 additional locations over the continental United States. The module tilt at all locations was 20 degrees. Results are given in Fig. 4 in two different forms. In the top panel, the plot displays the relative increase in energy produced by the module with mirror 5 compared to the module with the glass ARC. In the bottom panel, the plot shows the irradiance-weighted, time-averaged temperature difference between the modules.

Regardless of the location, the module with mirror 5 produces between 1.24% and 1.32% more energy than the one with the conventional glass ARC. Despite differences in irradiance, solar position, and the fraction of diffuse light compared to direct, the relative performance of the module does not exhibit significant variation.

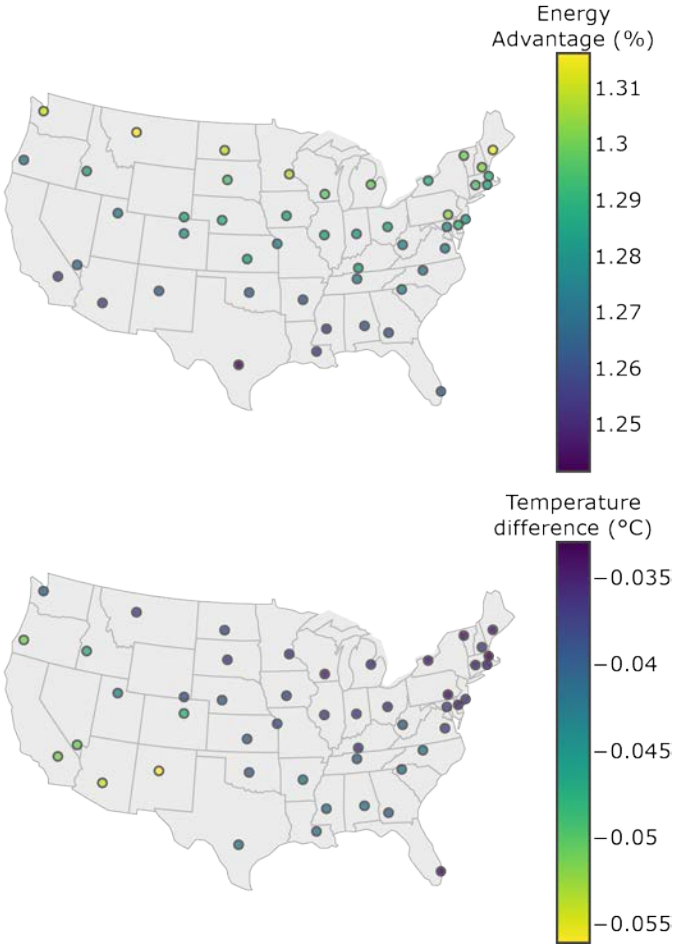

Fig. 4 (Top) Plot of relative increase in energy output for a module with mirror 5 compared to a module with a conventional glass ARC. Each dot represents a full-year simulation at that location. (Bottom) Plot of irradiance weighted temperature difference between a module with mirror 5 and a module with a conventional glass ARC. Each dot represents a full-year simulation at that location.

Fig. 4 shows that the cloudy, high-latitude areas generally show better relative performance for mirror 5, while sunny, low-latitude areas show worse relative performance. The major factor affecting optical module performance as geographic location changes is changing angle- of-incidence distribution, which, in turn, is affected by the module tilt and the amount of diffuse light. The lower the module tilt as compared to the latitude and the greater the fraction of diffuse light, the greater the fraction of sunlight incident between 40-60 degrees away from normal incidence (see supporting information of [2]). At these angles, these mirrors typically have better antireflection and closer alignment of the reflection turn-on with the bandgap, as can be seen for mirror 5 in Fig. 3. The result is slightly higher overall performance compared to a location where more light is incident at near-normal incidence. It must be emphasized that this trend holds only for mirrors designed to operate at all angles of incidence. Mirrors designed to work at near normal

incidence may not perform as well under more oblique angle radiation.

In terms of irradiance-weighted temperature difference, the module with mirror 5 operated at between 0.03°C and 0.06°C colder than the module with the conventional glass ARC. This is a small decrease, but notable given that the module with mirror 5 simultaneously produced ~1.28% more power. If the 1.28% power increase came without any thermal management, we expect that the module temperature would increase by ~0.29°C. One expects that in high irradiance areas, the temperature difference would rise, while in low irradiance areas the temperature difference would fall. This trend which is borne out in Fig. 4, and illustrates the importance of spectrally selective sub-bandgap reflectors for solar module performance in high-irradiance areas.

IV. Conclusion

Spectrally selective multilayer coatings provide an excellent opportunity to simultaneously increase module energy output while decreasing module temperature. Suitably designed coatings need not have more than ~10 layers, as in this study the more complex coatings did not outperform simpler ones in full-year simulations of module temperature and power output. The mirrors maintain similar performance even if the angular distribution of sunlight changes due to a shift in geographic location or cloudiness. Our best mirror, requiring only nine layers, allows for ~1.28% more annual energy production than a conventional glass ARC regardless of the location of the module in the continental United States, and reduces module operating temperature by 0.03°C to 0.06°C.

Acknowledgement

We thank Dana Dement for assistance with spectroscopic ellipsometry. Part of this work was carried out in the College of Science and Engineering Characterization Facility, University of Minnesota, which has received capital equipment funding from the NSF through the UMN MRSEC program under Award Number DMR-1420013. Part of this work was carried out in the College of Science and Engineering Minnesota Nano Center, University of Minnesota, which receives partial support from NSF through the NNIN program.

This work was authored in part by Alliance for Sustainable Energy, LLC, the manager and operator of the National Renewable Energy Laboratory for the U.S. Department of Energy (DOE) under Contract No. DE-AC36-08GO28308. Funding provided by the U.S. Department of Energy's Office of Energy Efficiency and Renewable Energy (EERE) under Solar Energy Technologies Office (SETO) Agreement Number 30312. The views expressed in the article do not necessarily represent the views of the DOE or the U.S. Government. The U.S. Government retains and the publisher, by accepting the article for publication, acknowledges that the U.S. Government retains a nonexclusive, paid-up, irrevocable, worldwide license to publish or reproduce the published form of this work, or allow others to do so, for U.S. Government purposes.

References

[1] X. Sun, T. J. Silverman, Z. Zhou, M. R. Khan, P. Bermel, and M. A. Alam. "Optics-based approach to thermal management of photovoltaics: selective-spectral and radiative cooling," *IEEE J. Photovolt.*, vol. 7, no. 2, pp. 566-574, 2017.

[2] I. M. Slauch, M. G. Deceglie, T. J. Silverman, and V. E. Ferry. "Spectrally selective mirrors with combined optical and thermal benefit for photovoltaic module thermal management," *ACS Photonics*, vol. 5, no. 4, pp. 1528-1538, 2018.

[3] W. Li, Y. Shi, K. Chen, L. Zhu, and S. Fan. "A comprehensive photonic approach for solar cell cooling," *ACS Photonics*, vol. 4, no. 4, pp. 774-782, 2017.

[4] U. Griesmann. *Optical Thin Film Toolbox for Octave & MATLAB*, 2015.

[5] A. V. Tikhonravov, M. K. Trubetskov, and G. W. DeBell. "Application of the needle optimization technique to the design of optical coatings," *Appl. Opt.*, vol. 35, no. 28, pp. 5493-5508, 1996.

[6] T. J Silverman, M. G. Deceglie, I. Subedi, N. J. Podraza, I. M. Slauch, V. E. Ferry, and I. Repins. "Reducing operating temperature in photovoltaic modules," *IEEE J. Photovolt.*, vol. 8, no. 2, pp. 532-540, 2018.

[7] L. V. Rodríguez-de Marcos, J. I. Larruquert, J. A. Méndez, and J. A. Aznárez. "Self-consistent optical constants of MgF_2, LaF_3, and CeF_3 films," *Opt. Mater. Express*, vol. 7, no. 3, pp. 989-1006, 2017.

[8] *Refractive Index Library, Material: Glass, Low-Fe Sodalime [Pil]*, Dataset, PV Lighthouse.

[9] S. John, C. Soukoulis, M. H. Cohen, and E. N. Economou. "Theory of electron band tails and the Urbach optical-absorption edge," *Phys. Rev. Lett.*, vol. 57, no. 14, pp. 1777-1780, 1986.

[10] I. Subedi, T. J Silverman, M. G. Deceglie, and N. J. Podraza. "Impact of infrared optical properties on crystalline Si and thin film CdTe solar cells," In *44th IEEE Photovoltaic Specialist Conference*, 2017.

[11] S. Wilcox and W. Marion. *Users Manual for TMY3 Data Sets*, Dataset NREL/TP-581-43156, National Renewable Energy Laboratory: Golden, CO (United States), 2008.

[12] I. Reda, and A. Andreas. *Solar Position Algorithm for Solar Radiation Applications*, Technical Report NREL/TP-560-34302, National Renewable Energy Laboratory: Golden, CO (United States), 2008.

[13] H. K. Raut, V. A. Ganesh, A. S. Nair, and S. Ramakrishna. "Anti-reflective coatings: a critical, in-depth review," *Energy Environ. Sci.*, vol. 4, no. 10, pp. 3779-3804, 2011.

[14] M. R. Vogt. "Development of Physical Models for the Simulation of Optical Properties of Solar Cell Modules," PhD, Leibniz University of Hanover: Hanover, Germany, 2015.